Temperature-dependent elasticity of Pb[(Mg_{0.33}Nb_{0.67})_{1-x}Ti_{x}]O_{3}

Sumudu Tennakoon, Joseph Gladden, Mainak Mookherjee, Tiglet Besara, and Theo Siegrist

Phys. Rev. B **96**, 134108 — Published 13 October 2017

DOI: 10.1103/PhysRevB.96.134108

09/18/2017

Temperature Dependent Elasticity of $Pb[(Mg_{0.33}Nb_{0.67})_{1-x}Ti_x]O_3$

Sumudu Tennakoon[1~], Joseph Gladden[2,3#], Mainak Mookherjee[1*], Tiglet Besara[4], and Theo Siegrist[4,5]

[1] Earth Materials Laboratory, Department of Earth, Ocean and Atmospheric Sciences, Florida State University, Tallahassee, FL 32306, USA.

~stennakoon@fsu.edu, *mmookherjee@fsu.edu

[2] Department of Physics and Astronomy, University of Mississippi, University, MS 38677, USA

#jgladden@olemiss.edu

[3] National Center for Physical Acoustics, University of Mississippi, University, MS 38677, USA

[4] National High Magnetic Field Laboratory, Tallahassee, FL 32310, USA.

[5]FAMU-FSU College of Engineering, Tallahassee, FL 32310, USA

Abstract

Relaxor ferroelectric materials, such as PMN-PT with generic stoichiometry $Pb[(Mg_{0.33}Nb_{0.67})_{1-x}Ti_x]O_3$ undergo a ferroelectric to paraelectric phase transition as a function of temperature. The exact transition characterized by Curie temperature (T_c) varies as a function of chemistry (x), i.e., the concentration of Ti. In this study, we investigated the structural phase transition by exploring the temperature dependence of the single crystal elastic properties of $Pb[(Mg_{0.33}Nb_{0.67})_{0.7}Ti_{0.3}]O_3$ i.e., $x \approx 0.3$. We used resonant ultrasound spectroscopy (RUS) to determine the elasticity at elevated temperatures, from which a $T_c = 398 \pm 5\,K$ for PMN-PT ($x \approx 0.3$) was determined. We report the full elastic constant tensor ($C_{ij} = \{C_{11}, C_{12}, C_{44}\}$), acoustic attenuation (Q^{-1}), longitudinal (V_P), and shear (V_S) sound velocities, and elastic

anisotropy of PMN-PT as a function of temperature for $400\ K < T < 871$ K. Temperature trends of the elastic constants C_{11}, C_{44} and bulk modulus indicate that at $T > T_c$ the material first stiffens and reaches maxima in the vicinity of the Burns temperature (T_b~673 K), followed by a more typical gradual softening of the elastic constants. Similar temperature dependent anomalies are also observed with anisotropy and Q^{-1}, with minima in the vicinity T_b. We used the temperature dependence of C_{ij}, Q^{-1}, V_P, V_S, and anisotropy to infer the evolution of polar nanoregions (PNRs) as the material evolved from $T > T_c$.

Introduction

Lead magnesium niobate-lead titanate (PMN-PT) is a relaxor ferroelectric material and belongs to a subfamily of lead-based complex-perovskites. Perovskites have ABO_3 stoichiometry, where the *A* sites have 12-fold coordination and the *B*-sites have 6-fold octahedral coordination. In PMN-PT perovskites, the Pb atoms are in the *A* site and the *B* site is either occupied by Ti atoms as in $PbTiO_3$ or by a pair of low and high valency atoms with a general stoichiometry of $Pb[(B_l^{\alpha+})_\delta\ (B_h^{\beta+})_{1-\delta}]O_3$ [1]. The subscript "*l*" in "B_l" refers to the low-valency sites and is typically occupied by Mg, Zn, Ni, Zr, In, Fe, Sc, Y cations. The subscript "*h*" in "B_h" refers to the high-valency sites and is typically occupied by Nb, Ta, and W cations [1]. The charge balance in the crystal structure is maintained by the relation $\delta.\alpha + (1-\delta).\beta = 4$. B_l and B_h sites in the $Pb(Mg_{0.33}Nb_{0.67})O_3$ crystal structure are occupied by Mg and Nb respectively i.e., with a δ of $1/3$. PMN-PT is a solid solution with a general stoichiometry of $Pb[(Mg_{0.33}Nb_{0.67})_{1-x}Ti_x]O_3$ where, $x = 0$ and 1 refers to the end members $Pb(Mg_{0.33}Nb_{0.67})O_3$ (PMN) and $PbTiO_3$ (PT) respectively. Single crystal of PMN-PT can be synthesized at high-temperatures (≈ 1300 K) [2].

Below the Curie temperature (T_c), uniformly aligned electric dipoles in relaxor ferroelectric materials are arranged to form several domains, which in turn generates a spontaneous polarization. Polarizations of these domains can be altered by application of an external electric field. At temperatures, greater than T_c, the ferroelectric phase transform to the paraelectric phase, accompanied by a reduction in the size of the polarized domains to randomly oriented polar nano-regions (PNRs). PNRs, however, do affect the bulk properties of the material such as elasticity [3,4]. At higher temperatures, i.e., T > T_b (T_b = Burns temperature), the PNRs are eventually fully depleted and the material becomes paraelectric. The Burns temperature for $Pb[(Mg_{0.33}Nb_{0.67})_{1-x}Ti_x]O_3$ with $x = 0$ and 0.30 is 623 K and 673 K respectively [5–7]. For $Pb[(Mg_{0.33}Nb_{0.67})_{1-x}Ti_x]O_3$ compositions with $x > 0.3$, T_b is slightly affected by varying x [8] and $T_b > T_c$ by ≈270 K. Relaxor ferroelectrics are often good piezoelectric materials below the T_c, with the temperature dependent dielectric response defined by a broad peak with a maximum at T_m, and is also dependent on frequency. This is in contrast to the well defined and sharp peak observed for regular ferroelectrics [9].

In the temperature-composition (T-x) diagram for PMN-PT, the relaxor PMN phase ($x=0$) is rhombohedral with *R3m* space group symmetry below the T_c [3,10–14], while the ferroelectric PT phase ($x=1.0$) is tetragonal with *P4mm* space group symmetry [3,10–13]. The composition range with $0.30 < x < 0.35$ is often described as the morphotropic phase boundary (MPB) of PMN-PT [3,10,11] and is characterized by the abrupt changes in the crystal structure and piezoelectric properties [3,15–18]. PMN-PT phases with monoclinic and orthorhombic space group symmetries have been reported in the vicinity of the MPB [19–22]. At T_c, the PMN-PT crystal undergoes a structural phase transition to cubic space group symmetry $Pm\bar{3}m$ [3]. This ferroelectric to paraelectric phase transition temperature varies linearly with composition (x). The ferroelectric-

paraelectric transition temperatures for the end members PMN and PT are 283 K and 765 K respectively [3,10,11], whereas the transition temperature in the vicinity of the MPB region is around 400 K [3,10–12,23]. The PMN-PT phases at and near the MPB region ($0.30 < x < 0.35$) have been extensively studied owing to their unusually large electromechanical properties, i.e., piezoelectric coefficients d_{33} =1500 - 2500 pC/N and electromechanical coupling factor of $k_{33} > 0.9$ [15,24]. PMN-PT crystals find applications in transducers in highly sensitive broadband acoustic devices, actuators, and energy harvesting devices [2,3,15].

It is well known, that structural phase transitions are often manifest themselves in the changes in elasticity [25–29]. Although PMN-PT is an extensively studied material, the temperature dependence of the single crystal elasticity of PMN-PT remains largely unexplored. Only the room temperature elasticity for PMN-PT has been reported [30–33] **(Table 1)**. Here, we explore the temperature dependent elasticity, elastic anisotropy, and acoustic attenuation of PMN-PT crystal across a wide range of temperatures (400- 871 K), and we relate our temperature dependent elasticity results to the structural changes associated with the ferroelectric transition in PMN-PT.

Materials and Methods

We obtained the PMN-PT crystals from the H.C. Materials Corporation. Unpolarized single crystals of PMN-PT were grown using the Bridgeman method [2,33]. We cut precise rectangular parallelepiped samples of dimensions of 0.3540(5) × 0.2580(5) × 0.1990(5) cm using South Bay Technologies 660 slow speed diamond wheel saw. We polished the sample faces using a lapping machine to a smooth optical quality surface. We used single crystal X-ray diffraction at National Magnetic High Field Laboratory, Florida State University to verify that the [001], [010],

and [001] crystal axes were oriented parallel to the axial directions of the rectangular parallelepiped. We used powder X-ray diffraction to determine the space group symmetry (*R3m*) and lattice parameters of the sample, which are $a = b = c = 4.01964(2)$ and $\alpha = \beta = \gamma = 89.894(4)$ (**Supplementary Figure SF1a** [34]). The mass of the sample is 0.1460(1) g and the corresponding density is 8.04(5) g cm^{-3}. The measured density agrees with a previous study on PMN-PT of similar composition [31]. We also determined the stoichiometry of the sample using an Energy Dispersive X-ray spectroscopy in a Scanning Electron Microscopy (SEM-EDS) at the Condensed Matter and Materials Physics Facility, Department of Physics, Florida State University. The PMN-PT sample used in our study has stoichiometry of $Pb[(Mg_{0.33}Nb_{0.66})_{0.7}Ti_{0.3}]O_3$.

We used Resonant Ultrasound Spectroscopy (RUS) at the National Center for Physical Acoustics (NCPA), University of Mississippi to determine the elastic constants in the temperature range of 293-871 K, by utilizing mechanical resonance spectra (MRS) of the solid sample. The MRS consists of a set of natural frequencies, which are influenced by the elastic constant tensor (C_{ij}), density (ρ), and geometry of the sample. The elastic constants are in turn influenced by the crystal structure. Resonance occurs when the excitation frequency (f) equals a natural frequency (f_0) of the sample. The vibrations are amplified approximately by the quality factor of the resonances ($Q = \frac{f_0}{\Delta f}$), where Δf is the full width at half maximum for the resonance frequency. The maximum number of modes observed in MRS is ~ 21, of which we used 16 modes across all temperatures for the determination of elastic constants. We predicted the normal mode frequencies f_i^{calc} ($i = 1,2, \ldots$) of the PMN-PT following the Rayleigh -Ritz method [26,28,35–39]. We use the least squares method to minimize ΔF, defined as $\sqrt{\frac{1}{N}\sum_{i=1}^{N}\left(\frac{f_i^{obs} - f_i^{calc}}{f_i^{meas}}\right)^2} \times 100\%$,

where the f_i^{obs} and f_i^{calc} are observed and calculated resonance frequencies We calculate the resonance frequencies based on initial guess of elastic constants (C_{ij}). Our MRS spectra have a $\Delta F < 0.45$ % (400-500 K) and it is ≈ 0.3 at T > 500 K. We determine the uncertainty for the elastic moduli (δC_{ij}) from the effective curvature ($\frac{df}{dC_{ij}}$) of the minima in elastic moduli. Our error-estimate for the elastic constants are: $\delta C_{11} < 2$ %, $\delta C_{12} < 3$ %, and $\delta C_{44} < 0.3$ %.

In the RUS experimental set-up, we placed our sample between two lithium niobate ($LiNbO_3$) piezoelectric transducers (**Supplementary Figure SF1b** [34]). A Stanford Research Systems (SRS) DS345 function generator was used to excite one of the transducer in contact with the sample with a sweeping sinusoidal signal. The other transducer was connected to an SRS SR844 lock-in amplifier that monitors the vibration response of the sample. A thermocouple is placed in proximity to the sample**.** The sample and the surrounding ceramic framework is placed in a fused quartz tube and then inserted in the high-temperature furnace (Carbolite MTF 12/28/250). In our high-temperature experiments, we maintained temperatures within ± 1 K using a proportional integral derivative controller. An inert gas flushing system is employed to maintain the oxygen content at low levels (< 20 ppm) to minimize oxidation reaction of the sample, transducer and electrical contacts [26,40].

At temperatures below 400 K, i.e., T< T_c, the MRS shows significant peak broadening and low signal to noise ratio (SNR) making it difficult to extract meaningful information on elastic constants at T< T_c. Hence, we conducted pulse-echo (PE) measurements on our PMN-PT sample to determine the elastic constant at room temperature [41,42]. We used an Olympus 5072PR pulsar-receiver to generate ultrasonic pulses (**Supplementary Figure SF1c** [34]). To measure the longitudinal wave speed (V_P), we used an ultrasonic gel to couple a 10 MHz longitudinal transducer (Olympus V112) to the sample. To measure the shear wave speed (V_S), we used

commercially available shear viscous gel to couple a 5 MHz shear transducer (Olympus V156) to the sample. We used a Tektronix TDS3000B digital oscilloscope to measure the pulse-echo signal in the time domain. We measured the wave speed along the [001] direction of the cubic PMN-PT crystal. We determined V_P and V_S using the relation between the travel time (Δt) and the sample thickness ($d = 2\ mm$) as $V = \frac{2d}{\Delta t}$. We derived elastic constants (C_{33}) and (C_{44}) from the measured speeds along [001] directions using the formulas: $V_{P[001]} = \sqrt{\frac{C_{33}}{\rho}}$ and $V_{S[001]} = \sqrt{\frac{C_{44}}{\rho}}$, where ρ is the density.

Results and Discussion

At room temperature, the symmetry of PMN-PT ($x \approx 0.3$) is pseudo-cubic [43] i.e., with three distinct elastic constants C_{11}, C_{12}, and C_{44}. We measured the longitudinal (V_P) and transverse (V_S) velocity along [001] direction and deduced C_{44} and C_{33} (where $C_{33} \approx C_{11}$) **(Table 1).** It is expected that at room temperature, i.e., T< T_c, the single crystal PMN-PT is twinned owing to the lowering of the symmetry to rhombohedral space group ($R3m$) from the cubic space group ($Pm\bar{3}m$). Thus, we examined the single crystal diffraction pattern of the PMN-PT ($x \approx 0.3$) crystal at room temperatures. We were, however, unable to observe distinct evidence of twinning based on the room temperature single crystal X-ray diffraction. The elasticity results of twinned crystals may require additional data analysis [44], we determined the elastic constants of PMN-PT ($x \approx 0.3$) at room temperature assuming an un-twinned crystals and our values are in good agreement with previous studies on PMN-PT from the MPB region **(Table 1)**. At higher temperatures, i.e., T> T_c the symmetry is cubic and the crystal becomes untwinned. We collected MRS of the PMN-PT ($x \approx 0.3$) crystal from room temperature (293 K) up to 871 K **(Figure 1)**.

In the temperature range of $373 - 423$ K, we observe an abrupt change in the MRS at $\sim 398 \pm 5$ K, this is defined as the Curie transition temperature (T_c) where the ferroelectric to paraelectric phase transition occurs in PMN-PT. This transition temperature compares favorably to the ferroelectric phase transition temperature (T_c) of PMN-PT with compositions $x \approx 0.3$ [10,11,23,45,46]. At $T > T_c$, we note a monotonic increase in the resonance mode frequencies (f_i) with the temperature indicating stiffening of the material. The temperature dependence of the f_i show a significant variation in their temperature maxima in the range $600 - 673$ K. We do not observe any hysteresis in f_i upon multiple heating and cooling cycles, i.e., the PMN-PT sample undergoes a reversible change in the explored temperature range.

In the temperature range of 400 K to 673 K, we observe a non-linear increase in the longitudinal (C_{11}) and shear elastic constants C_{44} by 40% and 33% respectively. In contrast, the off-diagonal elastic constant C_{12} decreases upon heating reaching a minimum at 493 ± 20 K and then increases upon further heating **(Figure 2).**

We define average acoustic energy loss for all the modes, $Q_{av}^{-1} = \frac{\sum_i^N Q_i^{-1}}{N}$, where Q_i^{-1} refers to acoustic energy loss of individual mode and N is the total number of modes considered in this study, i.e., 16. We identify three distinct regions marked: "1" "2" and "3" in the temperature dependence of the Q_{av}^{-1} **(Figure 2)**. The three distinct temperature regions relate to the dissipation of energy owing to the presence of randomly oriented polar nano-regions. In the region "1", i.e., $412\ K < T < 450$ K the Q_{av}^{-1} reduces by ~75%; in the region "2" i.e., $450\ \text{K} < T < T_b$, the Q_{av}^{-1} remains constant within 25 ± 5 % of the Q_{av}^{-1} at T = 412 K; and finally, in the region "3", at $T > T_b \sim 673\ K$, Q_{av}^{-1} increases linearly.

By examining the plots of the mode displacement field and the parity group (k value) of the mode, we categorized the measured sample resonance mode into modes related to torsion, flexure, shear, and dilation [35,36,47]. We labeled the resonant modes of PMN-PT as FZ-1: the lowest order flexure mode in the Z direction, SY-1: the lowest order shear mode in the Y direction, DO-1: the lowest order dilation mode, TO-1: the lowest order torsion mode **(Figure 1)**. We used the derivative $\frac{df}{dC_{ij}}$ $(ij = \{11, 12, 44\})$ of each mode to relate the dominant elastic constants, as the lower order resonance modes are often related to single elastic constant. For instance, the FX-1, FY-1, FZ-1, and DO-1 are likely to be related to C_{11}. The TO-1, TO-2, SX-1, and SZ-1 modes are likely to be related to the $C_{44,}$ Similarly, the higher order modes are often related to a combination of elastic constants. The TO-1, TO-2, SX-1, and SZ-1 modes related to C_{44} showed similar temperature dependences with maxima at 570 ± 20 K, whereas the modes FX-1, FY-1, FZ-1, and DO-1 modes related to C_{11} showed similar temperature dependences with maxima at 650 ± 20 K (**Figure 2**). The linear behavior of the elastic constants at the temperatures above T_b can be attributed to the lattice anharmonicity in the paraelectric phase of the material.

We calculated isotropic bulk modulus (K_H) and shear modulus (G_H) using the measured elastic constants, C_{ij}s following the Voigt-Reuss-Hill (VRH) approximations (**Table 1**) [48,49]. The Hill averaged bulk modulus (K_H) and shear modulus (G_H) for cubic crystals are defined as $K_H = \frac{1}{2}\,(K_V + K_R)$ and $G_H = \frac{1}{2}(G_V + G_R)$ where, the subscript "V" refers to Voigt averaged, $K_V = \frac{(C_{11} + 2C_{12})}{3}$, the subscript "R" refers to Reuss averaged, $K_R = \frac{1}{(3S_{11} + 6\,S_{12})}$, $G_V = \frac{(C_{11} - C_{12}) + 3\,C_{44}}{5}$, and $G_R = \frac{5}{4(S_{11} - S_{12}) + 3\,S_{44}}$. The components of the compliance tensor (S_{ij}) are obtained from $[S_{ij}] = [C_{ij}]^{-1}$. We used isotropic K_H and G_H values in the following equation

to calculate the Poisson's ratio $\nu = \frac{(3K_H - 2G_H)}{2(3K_H + G_H)}$. The isotropic Poisson ratio (ν) decreased in the temperature range of $400 - 530\,K$ with a minimum observed at 530 K. Above 530 K, ν gradually increases linearly (**Supplementary Figure SF2** [34]).

We used polycrystalline aggregate elastic moduli to determine the longitudinal, $V_P = \sqrt{\frac{K_H + \frac{4}{3}G_H}{\rho}}$ and shear, $V_S = \sqrt{\frac{G_H}{\rho}}$ sound wave velocities as functions of temperature (**Supplementary Figure SF2** [34]). In order to analyze the sound wave velocities as functions of propagating direction in the crystal, we applied the full elastic tensor of PMN-PT ($x \approx 0.3$) obtained from the RUS measurements in solving the Christoffel equation [50,51]:

$$\sum_{ij} \left[M_{ij} - V^2 \delta_{ij} \right] p_j = 0$$

where, V is sound velocity, $M_{ij} = \sum_{nm} k_n C_{ijkl} k_m$, $\delta_{ij} = \begin{cases} 1, & i = j \\ 0, & otherwise \end{cases}$, $\vec{k} = (k_1, k_2, k_3)$, are unit-vectors along propagation directions, and $\vec{p} = (p_1, p_2, p_3)$ are polarization vectors. A stereographic projection of longitudinal sound velocity (V_P), the two transverse shear velocities, V_{S1} and V_{S2} demonstrates the cubic space group symmetry of the PMN-PT crystal (**Figure 3)**. We also observed that the sound velocity anisotropies ($AV_P, AV_{S1}, and\ AV_{S2}$) of PMN-PT reduces asymptotically at higher temperature and exhibits minima at the Burns temperature, i.e., $T_b \approx$ 673 K **(Figure 3)**.

For the PMN-PT ($x \approx 0.3$) phase, at temperatures below T_c, <400 K, the microstructure consists of ferroelectric domains with spontaneous polarization. The size of these domains are often of micrometer scale [52] and they cause dissipation of acoustic energy which results in weakening of the resonance peaks in the MRS. The difficulty in acquiring elasticity measurement by the RUS method at temperatures below T_c is also known for several other relaxor ferroelectrics

including $Pb(In_{0.5}Nb_{0.5})O_3$-$Pb(Mg_{0.33}Nb_{0.67})O_3$-$PbTiO_3$ (PIN-PMN-PT) [27], $Ca_{0.28}Ba_{0.72}Nb_2O_6$ (CBN) [53,54], $LaAlO_3$ [55], and $KTa_{1-x}Nb_xO_3$ (KTN) [25]. In PMN-PT relaxor ferroelectrics, for compositions towards the PMN end i.e., between $x \approx 0.0$ and $x \approx 0.3$ as the temperature surpasses T_c, these ferroelectric domains are severely reduced and the crystal structure gradually transitions from the rhombohedral space group symmetry to a pseudo-cubic symmetry structure, which, eventually transitions to a cubic space group symmetry [10,56,57]. An ordinary ferroelectric material becomes paraelectric at $T > T_c$, but in the case of relaxors, polar nano-regions (PNRs) with randomly oriented local polarization exist at $T_c < T < T_b$ [5] **(Figure 2)**. These PNRs are reduced with increasing temperature, and at temperatures $T > T_b$, the PNRs eventually vanish and the crystal loses any local polarization. The T_b for PMN-PT is determined [5] based on the temperature dependence of the strain, thermal expansion coefficient, and the magnitude of the polarization. The transition from PNR to complete loss of polarization is well documented in the transition between region "2" and region "3" in the plot of Q_{av}^{-1} vs. temperature (**Figure 2**). The temperature dependence of elasticity in the PMN-PT from this study compares well with RUS results of other relaxor ferroelectrics including PIN-PMN-PT [27], CBN [54,53], and KTN [25] .

We compared the room temperature elasticity, i.e., bulk and shear moduli across the PMN-PT solid solution (**Figure 4a,b**). We note that the bulk modulus decreases from the PMN end member and reaches a minimum at the morphotropic phase boundary i.e., PMN-PT with $x = 0.3$, at $x > 0.3$, the bulk modulus is larger and then it reduces monotonically towards the PT ($x = 0.3$) (**Figure 4b**). The variation of shear modulus across PMN-PT solid solution shows a clear minimum at the morphotropic boundary i.e., PMN-PT with $x = 0.3$, both the end member

compositions i.e., PMN ($x = 0.0$) and PT ($x = 1.0$) have shear moduli greater than at MPB (**Figure 4b**).

The temperature dependence of these isotropic moduli is shown in (**Figure 4c)**. In the PMN-PT ($x = 0.3$) crystal, we observe that the bulk, K_H and shear, G_H moduli stiffens at high temperature up to $\approx T_b$, followed by a gradual softening. However, the maxima in the temperature dependence of the bulk, K_H and shear, G_H moduli occur at different temperatures of $673 \pm 20\ K$ and $623 \pm 20\ K$ respectively. We compared the high temperature elasticity of PMN-PT with previous studies on PMN using ultrasonic speed of sound measurements [58], Brillouin scattering [59,60] and RUS [14]. We note that the ferroelectric to paraelectric transition temperature (T_c) varies as a function of composition of PMN-PT, for instance for PMN ($x = 0.0$) and PMN-PT ($x = 0.3$), T_c is $270\ K$ and $398\ \pm 5\ K$ respectively. We note that the T_c increases from PMN to PT (**Figure 4a,c**). At the PMN end member the octahedral sites are occupied by both Mg and Nb cations. At T<T_c the Mg and Nb cations move along the [111] direction i.e., one 3-fold axis of the cube and lowers the cubic symmetry to a rhombohedral symmetry. As the Ti concentration increases in the octahedral site, the PMN-PT crystal structure stabilizes in the tetragonal space group symmetry at T<T_c owing to the displacement of Ti along the [001] direction. At T< T_c the morphotropic phase boundary is a special region in between the rhombohedral space group symmetry at the PMN rich end member and the tetragonal symmetry towards the PT rich end member. At MPB, the octahedral site in PMN-PT is almost half occupied by Nb (0.47), and the remaining half of the octahedral site is occupied by a combination of Ti (0.30) and Mg (0.23). Based on the temperature dependence of the bulk and shear moduli, the difference between elastic constants at T_b and T_c can be estimated. We find that the change in bulk (K) and shear (G) moduli are ≈ 18 and ≈ 24 GPa respectively for PMN-PT ($x = 0.3$) and

respectively. In comparison, the change in bulk (K) and shear (G) moduli are ≈ 10 and ≈ 20 GPa respectively for PMN ($x = 0$)[14,58–60]. The change in bulk (ΔK) and shear (ΔG) moduli is estimated by taking the difference between the bulk and shear moduli at temperatures between T_b and T_c and the linear extrapolation of the bulk and shear moduli fitted to the data at $T > T_b$. The change in bulk (ΔK) and shear (ΔG) moduli as a function of temperature is very nonlinear and can be adequately described by a power law,

$$\Delta C = A(T - T_f)^{\kappa},$$

where, ΔC represents ΔK or ΔG, A and κ are material constants, and T_f is a temperature where the nano polar domains freezes and T_f<T_C [55] (**Figure 4d**). So, in the composition region defined by $0.0 < x < 0.3$, we note that the addition of titanium into PMN i.e., increase in x, is likely to elevate the magnitude of elasticity change (ΔC) with the ferroelectric to paraelectric phase transition in PMN-PT.

Conclusions

We examined the temperature dependent ferroelectric to paraelectric transition of the PMN-PT ($x = 0.3$). Across the structural phase transition, the symmetry changes from rhombohedral to pseudo-cubic at T_c. Examining the temperature dependences of MRSs over the transition temperature range, we determined the ferroelectric transition temperature (T_c) of PMN-PT ($x = 0.3$) to be 398 ± 5 K. We measured the full set of elastic constants (C_{ij}) of the relaxor ferroelectric PMN-PT in the temperature range of $400 - 871$ K. The temperature evolution of the PMN-PT elastic moduli establish a significant stiffening in the temperature range $T_c < T < T_b$ followed by a gradual softening. In the temperature range $T_c < T < T_b$, the temperature dependences of the elastic constants C_{11}, C_{12}, and C_{44} behave in a distinct manner, likely related

to the differences in sensitivity of these elastic constants to the evolution of PNRs. We report that the maxima in C_{11} and isotropic bulk modulus (K), and the minimum of the sound wave anisotropy (AV_P, AV_S) correlates with the Burns temperature ($T_b \approx 673\ K$). We also detected an anomaly in the acoustic attenuation (Q^{-1}) with a broad minimum in the vicinity of T_b, followed by a linear increase at temperatures $T > T_b$. The nonlinear behavior of the elastic constants, acoustic attenuation, and elastic anisotropy of PMN-PT is attributed to the evolution of the PNRs at $T_c < T < T_b$ and their depletion at $T > T_b$.

Acknowledgments

ST and JG acknowledge National Center for Physical Acoustics, University of Mississippi. ST acknowledges the Graduate School Dissertation Fellowship, University of Mississippi in Spring 2016. ST and MM acknowledge National Science Foundation award # EAR-1639552 and EAR-1634422. TB and TS acknowledge support by the National Science Foundation under contract DMR-1625780. A part of this work was performed at the National High Magnetic Field Laboratory (NHMFL), which is supported by National Science Foundation Cooperative Agreement No. DMR-1157490, the State of Florida and the DOE.

References

[1] G. Jona, Franco, and Shirane, *Ferroelectric Crystals* (Pergamon Pres, New York, 1962).

[2] S. Zhang and F. Li, High Performance Ferroelectric Relaxor-$PbTiO_3$ Single Crystals: Status and Perspective, J. Appl. Phys., **111**, 31301 (2012).

[3] E. Araújo and E. Borges, in Recent Advances in Processing, Structural and Dielectric Properties of PMN-PT Ferroelectric Ceramics at Compositions Around the MPB, *Adv. Ceram. - Electr. Magn. Ceram. Bioceram. Ceram. Environ.* (InTech, 2011).

[4] A.A. Bokov and Z.-G. Ye, Recent Progress in Relaxor Ferroelectrics with Perovskite Structure, J. Mater. Sci., **41**, 31 (2006).

[5] R. Wongmaneerung, R. Guo, A. Bhalla, R. Yimnirun, and S. Ananta, Thermal Expansion Properties of PMN-PT Ceramics, J. Alloys Compd., **461**, 565 (2008).

[6] G. Burns and F.H. Dacol, Glassy Polarization Behavior in Ferroelectric Compounds $Pb(Mg_{1/3}Nb_{2/3})O_3$ and $Pb(Zn_{1/3}Nb_{2/3})O_3$, Solid State Commun., **48**, 853 (1983).

[7] P.M. Gehring, W. Chen, Z.-G. Ye, and G. Shirane, The Non-Rhombohedral Low-Temperature Structure of PMN–10% PT, J. Phys. Condens. Matter, **16**, 7113 (2004).

[8] J.-H. Ko, D.H. Kim, S. Tsukada, S. Kojima, A.A. Bokov, and Z.-G. Ye, Crossover in the Mechanism of Ferroelectric Phase Transition of$Pb[(Mg_{1/3}Nb_{2/3})_{1-x}Ti_x]O_3$ Single Crystals Studied by Brillouin Light Scattering, Phys. Rev. B, **82**, 104110 (2010).

[9] R.E. Cohen, Theory of Ferroelectrics: A Vision for the next Decade and beyond, J. Phys. Chem. Solids, **61**, 139 (2000).

[10] B. Noheda, D.E. Cox, G. Shirane, J. Gao, and Z.-G. Ye, Phase Diagram of the Ferroelectric Relaxor $(1-x)PbMg_{1/3}Nb_{2/3}O_3-xPbTiO_3$, Phys. Rev. B, **66**, 54104 (2002).

[11] Y. Guo, H. Luo, K. Chen, H. Xu, X. Zhang, and Z. Yin, Effect of Composition and Poling

Field on the Properties and Ferroelectric Phase-Stability of $Pb(Mg_{1/3}Nb_{2/3})O_3$–$PbTiO_3$ Crystals, J. Appl. Phys., **92**, 6134 (2002).

[12] Y. Guo, H. Luo, D. Ling, H. Xu, T. He, and Z. Yin, The Phase Transition Sequence and the Location of the Morphotropic Phase Boundary Region in $(1\text{-}x)[Pb(Mg_{1/3}Nb_{2/3})O_3]$-$x PbTiO_3$ Single Crystal, J. Phys. Condens. Matter, **15**, L77 (2003).

[13] J.H. Qiu, J.N. Ding, N.Y. Yuan, and X.Q. Wang, Phase Diagram of $(1-x)PbMg_{1/3}Nb_{2/3}O_3 -x PbTiO_3$ Single Crystals, J. Appl. Phys., **117**, 74101 (2015).

[14] M.A. Carpenter, J.F.J. Bryson, G. Catalan, S.J. Zhang, and N.J. Donnelly, Elastic and Anelastic Relaxations in the Relaxor Ferroelectric $Pb(Mg_{1/3}Nb_{2/3})O_3$□: II. Strain–order Parameter Coupling and Dynamic Softening Mechanisms, J. Phys. Condens. Matter, **24**, 45902 (2012).

[15] D. Fu, H. Taniguchi, M. Itoh, and S. Mori, $Pb(Mg_{1/3}Nb_{2/3})O_3$ (PMN) Relaxor: Dipole Glass or Nano-Domain Ferroelectric?, Adv. Ferroelectr., **3**, 8 (2012).

[16] F. Cordero, Elastic Properties and Enhanced Piezoelectric Response at Morphotropic Phase Boundaries, Materials (Basel)., **8**, 8195 (2015).

[17] Y. Chen, K.H. Lam, D. Zhou, Q. Yue, Y. Yu, J. Wu, W. Qiu, L. Sun, C. Zhang, H. Luo, H.L.W. Chan, and J. Dai, High Performance Relaxor-Based Ferroelectric Single Crystals for Ultrasonic Transducer Applications, Sensors (Basel)., **14**, 13730 (2014).

[18] M. Ahart, A. Asthagiri, Z.-G. Ye, P. Dera, H. Mao, R.E. Cohen, and R.J. Hemley, Brillouin Scattering and Molecular Dynamics Study of the Elastic Properties of $Pb(Mg_{1/3}Nb_{2/3})O_3$, Phys. Rev. B, **75**, 144410 (2007).

[19] M. Ghasemifard, S.M. Hosseini, and G.H. Khorrami, Synthesis and Structure of PMN-PT Ceramic Nanopowder Free from Pyrochlore Phase, Ceram. Int., **35**, 2899 (2009).

[20] W.D. Dong, P. Finkel, A. Amin, and C.S. Lynch, Giant Electro-Mechanical Energy Conversion in [011] Cut Ferroelectric Single Crystals, Appl. Phys. Lett., **100**, 1 (2012).

[21] Y. Lu, D.Y. Jeong, Z.Y. Cheng, Q.M. Zhang, H.S. Luo, Z.W. Yin, and D. Viehland, Phase Transitional Behavior and Piezoelectric Properties of the Orthorhombic Phase of $Pb(Mg_{1/3}Nb_{2/3})O_3$-$PbTiO_3$ Single Crystals, Appl. Phys. Lett., **78**, 3109 (2001).

[22] A.K. Singh, D. Pandey, and O. Zaharko, Powder Neutron Diffraction Study of Phase Transitions in and a Phase Diagram of $(1-x)[Pb(Mg_{1/3}Nb_{2/3})O_3]$-$xPbTiO_3$, Phys. Rev. B, **74**, 24101 (2006).

[23] O. Noblanc, P. Gaucher, and G. Calvarin, Structural and Dielectric Studies of $Pb(Mg_{1/3}Nb_{2/3})O_3$–$PbTiO_3$ Ferroelectric Solid Solutions around the Morphotropic Boundary, J. Appl. Phys., **79**, 4291 (1996).

[24] H. Fu and R. Cohen, Polarization Rotation Mechanism for Ultrahigh Electromechanical Response in Single-Crystal Piezoelectrics, Nature, **403**, 281 (2000).

[25] O. Svitelskiy, A. V. Suslov, J.B. Betts, A. Migliori, G. Yong, and L.A. Boatner, Resonant Ultrasound Spectroscopy of $KTa_{1-X}Nb_xO_3$ Ferroelectric Relaxor Crystals, Phys. Rev. B - Condens. Matter Mater. Phys., **78**, 1 (2008).

[26] G. Li and J.R. Gladden, High Temperature Resonant Ultrasound Spectroscopy: A Review, Int. J. Spectrosc., **2010**, 1 (2010).

[27] G.F. Nataf, Q. Li, Y. Liu, R.L. Withers, S.L. Driver, and M.A. Carpenter, Ferroelastic Aspects of Relaxor Ferroelectric Behaviour in $Pb(In_{1/2}Nb_{1/2})O_3$ -$Pb(Mg_{1/3}Nb_{2/3})O_3$ -$PbTiO_3$ Perovskite, J. Appl. Phys., **113**, 124102 (2013).

[28] R.G. Leisure and F.A. Willis, Resonant Ultrasound Spectroscopy, J. Phys. Condens. Matter, **9**, 6001 (1997).

[29] A. Migliori and T.W. Darling, Resonant Ultrasound Spectroscopy for Materials Studies and Non-Destructive Testing, Ultrasonics, **34**, 473 (1996).

[30] X. Liu, S. Zhang, J. Luo, T.R. Shrout, and W. Cao, Complete Set of Material Constants of $Pb(In_{1/2}Nb_{1/2})O_3$–$Pb(Mg_{1/3}Nb_{2/3})O_3$–$PbTiO_3$ Single Crystal with Morphotropic Phase Boundary Composition, J. Appl. Phys., **106**, 74112 (2009).

[31] H. Cao, V.H. Schmidt, R. Zhang, W. Cao, and H. Luo, Elastic, Piezoelectric, and Dielectric Properties of $0.58Pb(Mg_{1/3}Nb_{2/3})O_3$-$0.42PbTiO_3$ Single Crystal, J. Appl. Phys., **96**, 549 (2004).

[32] R. Zhang, in Elastic, Dielectric and Piezoelctric Coefficients of Domain Engineered $0.70Pb(Mg_{1/3}Nb_{2/3})O_3$-$0.30PbTiO_3$ Single Crystal, *AIP Conf. Proc.* (AIP, 2002), pp. 188–197.

[33] J. Luo, W. Hackenberger, S. Zhang, and T.R. Shrout, Elastic, Piezoelectric and Dielectric Properties of PIN-PMN-PT Crystals Grown by Bridgman Method, Proc. - IEEE Ultrason. Symp., 261 (2008).

[34] See Supplemental Material at [URL] for Powder X-Ray Diffraction Data, High-Temperature Resonant Ultrasound Spectroscopy (RUS), Pulse-Echo Experimental Setup, and Temperature Dependence of Sound Wave Velocities and Poisson's Ratio.

[35] I. Ohno, Free Vibration of a Rectangular Parallelepiped Crystal and Its Application to Determination of Elastic Constants of Orthorhombic Crystals., J. Phys. Earth, **24**, 355 (1976).

[36] W.M. Visscher, A. Migliori, T.M. Bell, and R.A. Reinert, On the Normal Modes of Free Vibration of Inhomogeneous and Anisotropic Elastic Objects, J. Acoust. Soc. Am., **90**, 2154 (1991).

[37] O.O.L. Anderson, Rectangular Parallelepiped resonance-A Technique of Resonance Ultrasound and Its Applications to the Determination of Elasticity at High Temperatures, J. Acoust. Soc. Am., **91**, 2245 (1992).

[38] A. Migliori and J.D. Maynard, Implementation of a Modern Resonant Ultrasound Spectroscopy System for the Measurement of the Elastic Moduli of Small Solid Specimens, Rev. Sci. Instrum., **76**, 121301 (2005).

[39] H.H. Demarest, Cube-Resonance Method to Determine the Elastic Constants of Solids, J. Acoust. Soc. Am., **49**, 768 (1971).

[40] G. Li, High Temperature Resonant Ultrasound Spectroscopy Studies of Thermoelectrics and Other Novel Materials, University of Mississippi, University, Mississppi, USA, 2010.

[41] A. Lopez-Sanchez and L.W. Schmerr, Characterization of an Ultrasonic Transducer in a Pulse-Echo Setup, AIP Conf. Proc., **820 I**, 900 (2006).

[42] C. Pantea, D.G. Rickel, A. Migliori, R.G. Leisure, J. Zhang, Y. Zhao, S. El-Khatib, and B. Li, Digital Ultrasonic Pulse-Echo Overlap System and Algorithm for Unambiguous Determination of Pulse Transit Time, Rev. Sci. Instrum., **76**, 114902 (2005).

[43] H. King, S. Ferguson, D.F. Waechter, and S.E. Prasad, in An X-Ray Diffraction Study of PMN–PT Ceramics near the Morphotropic Phase Boundary, *Proc. ICONS 2002. Int. Conf. Sonar – Sensors Syst.* (2002).

[44] J. Erhart and W. Cao, Effective Material Properties in Twinned Ferroelectric Crystals, J. Appl. Phys., **86**, 1073 (1999).

[45] B. Noheda, Structure and High-Piezoelectricity in Lead Oxide Solid Solutions, Curr. Opin. Solid State Mater. Sci., **6**, 27 (2002).

[46] M. Sepliarsky and R.E. Cohen, First-Principles Based Atomistic Modeling of Phase

Stability in PMN-xPT., J. Phys. Condens. Matter, **23**, 435902 (2011).

[47] A. Migliori and J.L. Sarrao, *Resonant Ultrasound Spectroscopy: Applications to Physics, Materials Measurements, and Nondestructive Evaluation* (Wiley-VCH, 1997).

[48] D.H. Chung and W.R. Buessem, The Voigt-Reuss-Hill (VRH) Approximation and the Elastic Moduli of Polycrystalline ZnO, TiO2 (Rutile), and α-Al_2O_3, J. Appl. Phys., **39**, 2777 (1968).

[49] R. Hill, The Elastic Behaviour of a Crystalline Aggregate, Proc. Phys. Soc. Sect. A, **65**, 349 (1952).

[50] J.W. Jaeken and S. Cottenier, Solving the Christoffel Equation: Phase and Group Velocities, Comput. Phys. Commun., **207**, 445 (2016).

[51] F.I. Fedorov, *Theory of Elastic Waves in Crystals* (Springer US, Boston, MA, 1968).

[52] S. Zhang, F. Li, N.P. Sherlock, J. Luo, H.J. Lee, R. Xia, R.J. Meyer, W. Hackenberger, and T.R. Shrout, Recent Developments on High Curie Temperature PIN-PMN-PT Ferroelectric Crystals., J. Cryst. Growth, **318**, 846 (2011).

[53] C.S. Pandey, J. Schreuer, M. Burianek, and M. Mühlberg, Anomalous Elastic Behavior of Relaxor Ferroelectric Ca0.28Ba0.72Nb2O6 Single Crystals, Phys. Rev. B, **84**, 174102 (2011).

[54] C.S. Pandey, J. Schreuer, M. Burianek, and M. Mühlberg, Relaxor Behavior of $Ca_xBa_{1-x}Nb_2O_6$ ($0.18 \leq x \leq 0.35$) Tuned by Ca/Ba Ratio and Investigated by Resonant Ultrasound Spectroscopy, Phys. Rev. B - Condens. Matter Mater. Phys., **87**, 0 (2013).

[55] M.A. Carpenter, A. Buckley, P.A. Taylor, and T.W. Darling, Elastic Relaxations Associated with the Pm3m –R3c Transition in $LaAlO_3$: III. Superattenuation of Acoustic Resonances, J. Phys. Condens. Matter, **22**, 35405 (2010).

[56] W. Ren, L. Han, R. Wicks, G. Yang, and B.K. Mukherjee, in Electric-Field-Induced Phase Transitions of <001>-Oriented $Pb(Mg_{1/3}Nb_{2/3})O_3$ -$PbTiO_3$ Single Crystals, *Smart Struct. Mater. 2005 Act. Mater. Behav. Mech.*, edited by W.D. Armstrong (2005), p. 272.

[57] L. Bellaiche and D. Vanderbilt, Intrinsic Piezoelectric Response in Perovskite Alloys: PMN-PT versus PZT, Phys. Rev. Lett., **83**, 1347 (1999).

[58] G.A. Smolenskii, N.K. Yushin, and S.I. Smirnov, Acoustic Properties of the Lead Magnoniobate Crystal as a Ferroelectric with a Smeared Phase Transition Region, Fiz. Tverd. Tela, **27**, 801 (1985).

[59] A.I. Fedoseev and S.G. Lushnikov, Elastic Properties of Cubic Relaxor Ferroelectrics, Bull. Russ. Acad. Sci. Phys., **72**, 1436 (2008).

[60] S.G. Lushnikov, A.I. Fedoseev, S.N. Gvasaliya, and S. Kojima, Anomalous Dispersion of the Elastic Constants at the Phase Transformation of the $PbMg_{1/3}Nb_{2/3}O_3$ Relaxor Ferroelectric, Phys. Rev. B, **77**, 104122 (2008).

[61] A.G. Kalinichev, J.D. Bass, B.N. Sun, and D.A. Payne, Elastic Properties of Tetragonal PbTiO3 Single Crystals by Brillouin Scattering, J. Mater. Res., **12**, 2623 (1997).

[62] M.K. Fig, MATLAB Software Calculates Resonant Frequencies and Mode Shapes for RUS, https://www.mathworks.com/matlabcentral/fileexchan (2008).

[63] S.W. Choi, R.T.R. Shrout, S.J. Jang, and A.S. Bhalla, Dielectric and Pyroelectric Properties in the $Pb(Mg_{1/3}Nb_{2/3})O_3$ -$PbTiO_3$ System, Ferroelectrics, **100**, 29 (1989).

[64] J.B. Li, G. Rao, G. Liu, J. Chen, L. Lu, X. Jing, S. Li, and J. Liang, Structural Transition in Unpoled (1 - *x*)PMN-*x*PT Ceramics near the Morphotropic Boundary, J. Alloys Compd., **425**, 373 (2006).

Table 1: Room temperature elastic constants (C_{ij}) across the PMN-PT solid solutions and from this study PMN-PT ($x \approx 0.3$). The elastic constants are reported in GPa. PE refers to pulse-echo and RUS refers to Resonant Ultrasound Spectroscopy.

	C_{11}	C_{12}	C_{13}	C_{33}	C_{44}	C_{66}	K_H	G_H	Source
PT ($x = 1.00$)	237	90	70	60	69	104	85	55	[61]
PMN ($x = 0.00$)	156	76			69		103	55	[18]
PMN-PT ($x = 0.29$)	124	111	104	108	63	35	93	30	[33]
PMN-PT ($x = 0.30$)	117	103	101	108	71	66	105	29	[32]
PMN-PT ($x = 0.33$)	115	103	102	103	69	66	104	25	[31]
PMN-PT ($x = 0.42$)	175	85	83	105	28	80	102	37	[31]
PMN-PT ($x \approx 0.30$)									
293 K				124.0	62.5				This work (PE)
PMN-PT ($x \approx 0.30$)									This work (RUS)
412 K	134.2	89.4			66.3		104.4	43.0	
443 K	157.8	87.7			74.5		111.1	55.0	
473 K	167.5	83.2			78.0		111.3	60.9	
493 K	174.4	83.9			77.8		114.1	62.6	
513 K	177.3	83.4			78.4		114.7	63.8	
572 K	183.3	84.7			78.8		117.6	65.3	
594 K	184.6	85.3			78.8		118.4	65.5	
671 K	185.7	86.1			78.5		119.3	65.4	
771 K	184.3	85.9			78.0		118.7	64.8	
872 K	181.5	85.6			77.0		117.6	63.7	

Figure Captions

Figure 1: (**a**) Temperature dependence of the first ten mechanical resonance frequencies (**b**) Temperature evolution of MRS from 290-823 K. For the PMN-PT sample ($x \approx 0.3$) explored in this study, a distinct transition in the temperature dependence of MRS is observed at around ~400 K, i.e., (T_c). Mode displacement plots [62] of first five resonance modes of the PMN-PT sample are also shown and indicated by arrows with the corresponding modes in (**b**).

Figure 2: Temperature dependence of C_{11}, C_{12}, C_{44}, and acoustic energy loss (Q_{av}^{-1}) of the same sample measured in two different temperature cycles. Also shown are the elastic constants for PMN (x=0.0) [14,58]. The two "grey and white" shaded regions shown in the figure indicates the ferroelectric to paraelectric transition with T_c for PMN and for PMN-PT. The T_c for PMN is ~ 270 K whereas the T_c for PMN is ~ 398 K.

Figure 3: (**a**) The plot shows the temperature dependence of the sound velocity anisotropy: AV_P, AV_{S1}, and AV_{S2}. We define the anisotropy $AV_P = \frac{200\times(V_{Pmax}-V_{Pmin})}{(V_{Pmax}+V_{Pmin})}$; and $AV_S = \frac{200\times(V_{Smax}-V_{Smin})}{(V_{Smax}+V_{Smin})}$; The inset shows the inflection in AV_P at the Burns temperature, T_b (**b**), (**c**), and (**d**) are the stereographic plots of the directional dependence of sound velocities: V_p, V_{s1}, V_{s2} at 412 K.

Figure 4: **(a)** Temperature-composition ($T - x$) phase diagram for PMN-PT with a stoichiometry $Pb[(Mg_{0.33}Nb_{0.67})_{1-x}Ti_x]O_3$. The phase diagram is subdivided based on the space group symmetry of the PMN-PT crystals- "C" refers to the cubic space group symmetry ($Pm\bar{3}m$), "R" refers to rhombohedral space group symmetry (*R3m*), "T" refers to tetragonal space group symmetry (*P4mm*) and "MPB" refers to morphotropic phase boundary which is attributed to monoclinic phases (*Bm* and *Pm*) [13] . The region. "PC"

refers to pseudo-cubic where $a = b = c$ and $\alpha = \beta = \gamma \lesssim 90$ [43]. The phase transition temperatures shown in the figure are from previous studies including X-ray diffraction (XRD) [10,11,43,63,64], dielectric measurements (DM) [11,23,63], and molecular dynamics (MD) simulations [46]. The shaded region extended up to x=0.5 indicates the MPB determined from MD [46]. Insert shows the crystal structure of a PMN-PT phase with cubic space group symmetry ($Pm\bar{3}m$). Dashed lines indicates the compositional variation of Burns temperature (T_b) [5,7]. **(b)** Bulk (K) and shear (G) moduli as a function of x. Room temperature K and G **(Table 2)** are connected with dashed lines. Color scale indicates the temperatures. **(c)** Bulk (K) and shear (G) moduli of PMN (x =0) [58] and PMN-PT (x =0.3) as a function of temperature. T_c for PMN and PMN-PT (x =0.3) is also marked in the plot. **(d)** ΔK and shear ΔG as a function of temperature. The blue and red lines represent fits $[A(T - T_f)^{\kappa}]$ to the ΔK and ΔG with $T_f = 380\ K$ [22]. The fitted parameter A for ΔK and ΔG are -499 and -2974 GPa respectively. The fitted parameter K for ΔK and ΔG are -0.96 and -1.36 respectively. The two "grey and white" shaded regions shown in the figure indicates ferroelectric to paraelectric transition with the T_c for PMN and for PMN-PT.

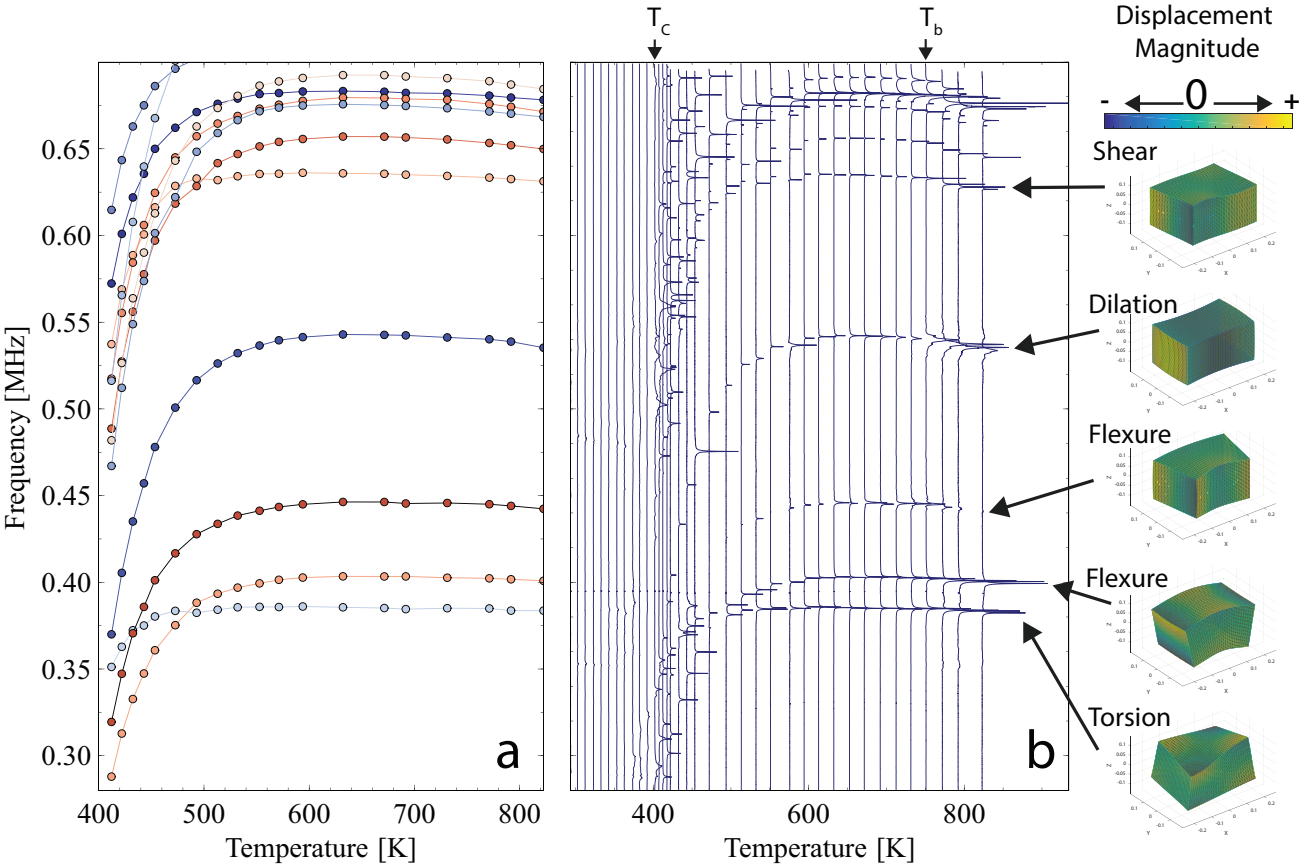

Figure 1 BE13263 18SEP2017

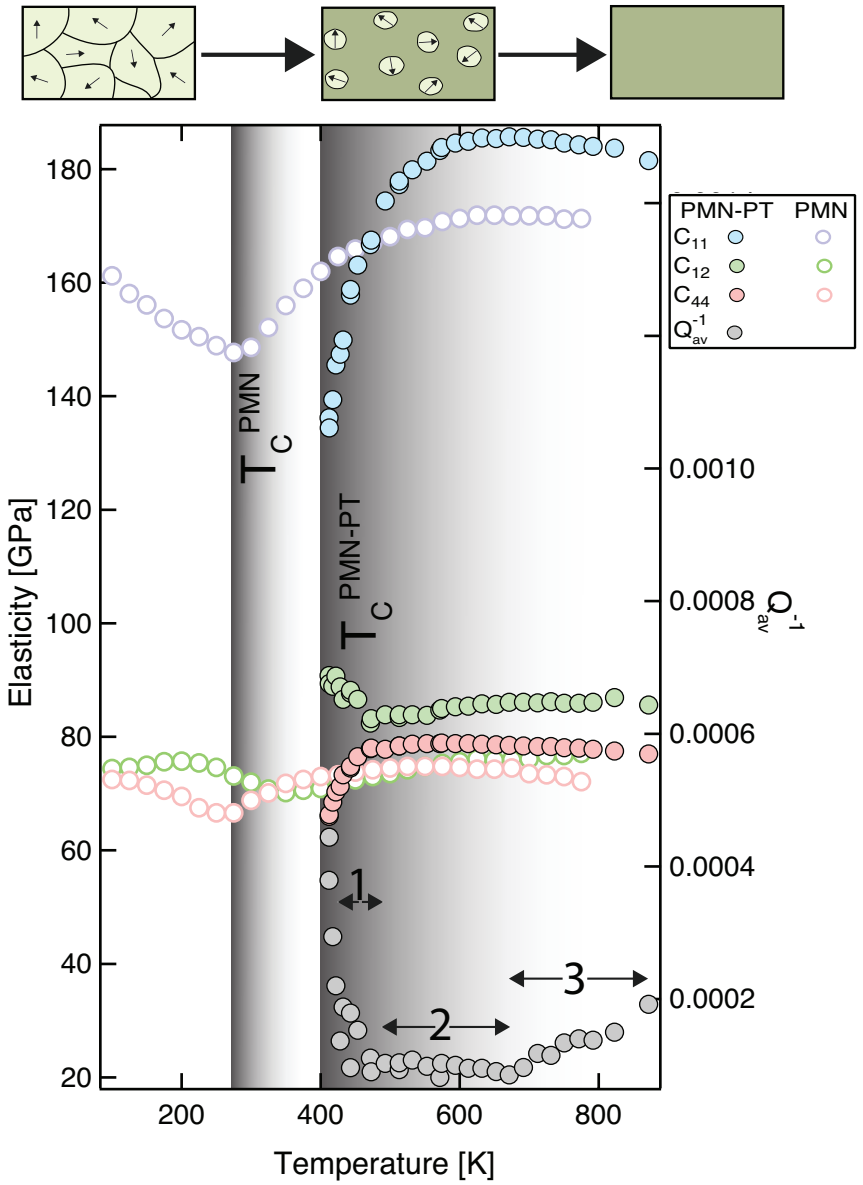

Figure 2 BE13263 18SEP2017

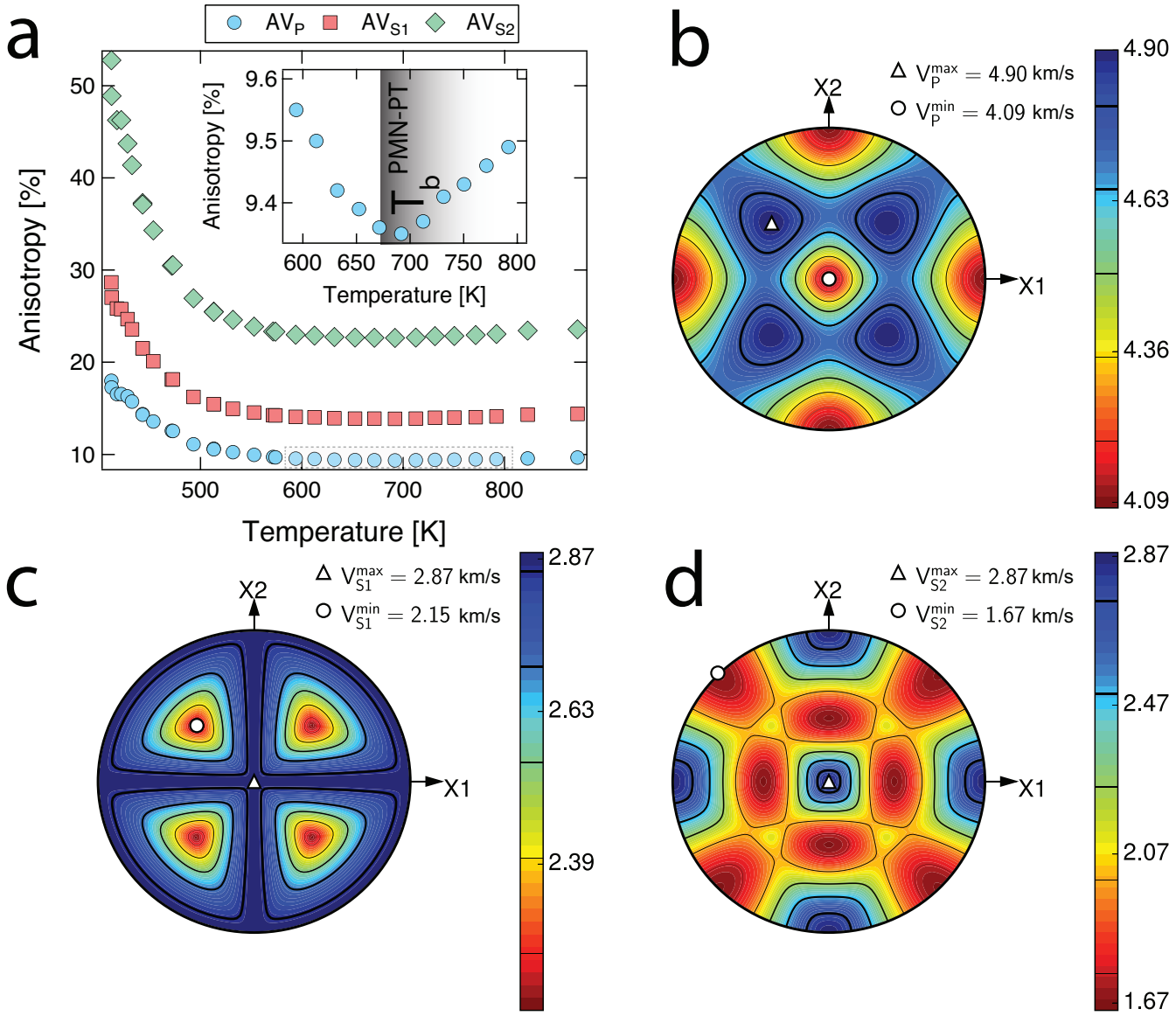

Figure 3 BE13263 18SEP2017

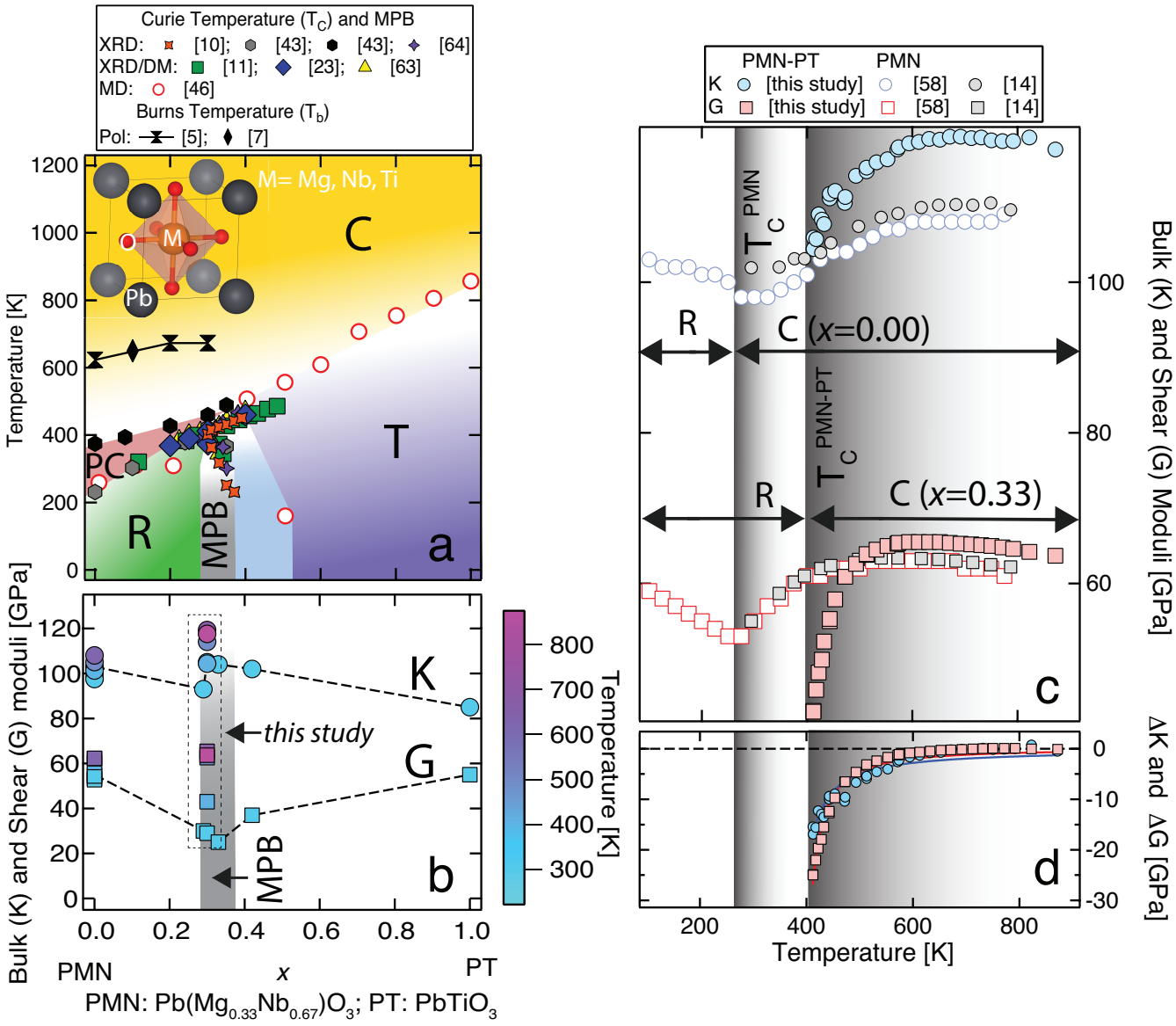

Figure 4 BE13263 18SEP2017